



Maximizing electrical activation of ion-implanted Si in In_{0.53}Ga_{0.47}As

A. G. Lind, N. G. Rudawski, N. J. Vito, C. Hatem, M. C. Ridgway, R. Hengstebeck, B. R. Yates, and K. S. Jones

Citation: [Applied Physics Letters](#) **103**, 232102 (2013); doi: 10.1063/1.4835097

View online: <http://dx.doi.org/10.1063/1.4835097>

View Table of Contents: <http://scitation.aip.org/content/aip/journal/apl/103/23?ver=pdfcov>

Published by the [AIP Publishing](#)



Re-register for Table of Content Alerts

Create a profile.



Sign up today!



Maximizing electrical activation of ion-implanted Si in $\text{In}_{0.53}\text{Ga}_{0.47}\text{As}$

A. G. Lind,^{1,a)} N. G. Rudawski,² N. J. Vito,¹ C. Hatem,³ M. C. Ridgway,⁴ R. Hengstebeck,⁵ B. R. Yates,¹ and K. S. Jones¹

¹Department of Materials Science and Engineering, University of Florida, Gainesville, Florida 32611, USA

²Major Analytical Instrumentation Center, University of Florida, Gainesville, Florida 32611, USA

³Applied Materials, Gloucester, Massachusetts 01930, USA

⁴Department of Electronic and Materials Engineering, Research School of Physical Sciences and Engineering, Australian National University, Canberra, ACT 0200, Australia

⁵Evans Analytical Group, East Windsor, New Jersey 08520, USA

(Received 11 September 2013; accepted 24 October 2013; published online 2 December 2013)

A relationship between the electrical activation of Si in ion-implanted $\text{In}_{0.53}\text{Ga}_{0.47}\text{As}$ and material microstructure after ion implantation is demonstrated. By altering specimen temperature during ion implantation to control material microstructure, it is advanced that increasing sub-amorphizing damage (point defects) from Si^+ implantation results in enhanced electrical activation of Si in $\text{In}_{0.53}\text{Ga}_{0.47}\text{As}$ by providing a greater number of possible sites for substitutional incorporation of Si into the crystal lattice upon subsequent annealing. © 2013 AIP Publishing LLC.

[<http://dx.doi.org/10.1063/1.4835097>]

Scaling limits for future complementary metal-oxide-semiconductor (CMOS) devices have stimulated a renewed interest in alternate channel materials.¹ In particular, there is great interest in the use of III-V compound semiconductors for n-type field-effect transistors because of the much larger electron mobilities compared to Si or Ge.² $\text{In}_{0.53}\text{Ga}_{0.47}\text{As}$ is of particular research interest due to the reported charge carrier mobilities as well as the ability to grow lattice-matched, high quality single-crystal $\text{In}_{0.53}\text{Ga}_{0.47}\text{As}$ on widely available InP substrates.³ However, one of the biggest challenges associated with the integration of III-V compound semiconductors in CMOS devices is the low solubility of ion-implanted dopants in III-V semiconductors relative to Si or Ge.⁴ Si is a promising n-type dopant in $\text{In}_{0.53}\text{Ga}_{0.47}\text{As}$ given its low diffusivity and higher reported solubility compared to other n-type dopants, such as S, Se, and Te.⁴ Yet, the activation of ion-implanted Si in $\text{In}_{0.53}\text{Ga}_{0.47}\text{As}$ remains poorly understood. It is known that avoiding amorphization by increasing the implantation temperature results in higher dopant activation in III-V compound semiconductors; however, the origin of this behavior is unclear, particularly since minimal structural characterization was performed in prior work.^{5–7} This study builds on the previous work exploring the effect of elevated specimen temperature during Si^+ -implantation by using a larger range of implant temperatures as well as more exhaustive characterization techniques comparing as-implanted morphology with post anneal activation of Si in InGaAs. The results suggest there is a correlation between the post ion implantation damage distribution and the subsequent electrical activation upon annealing.

Commercially available (001) InP wafers with 300 nm of epitaxial, lattice-matched $\text{In}_{0.53}\text{Ga}_{0.47}\text{As}$ were used for this work. Specimens were Si^+ -implanted at 20 keV to a dose of $6.0 \times 10^{14} \text{ cm}^{-2}$ with the specimen temperature maintained at 20–300 °C during implantation (implantation

temperature); the specimen tilt was set to 7° with respect to the incoming ion beam to minimize channeling effects. All specimens were annealed using rapid thermal annealing (RTA) at 750 °C (annealing temperature) for 5 s in N_2 ambient to activate the implanted Si dopant. Prior to annealing, all specimens were encapsulated with 15 nm of a protective Al_2O_3 layer deposited using atomic layer deposition to prevent surface degradation upon annealing.^{8,9} The encapsulating Al_2O_3 layer was then selectively removed by etching with 49% HF prior to electrical characterization. Electrical characterization of annealed specimens was performed using Van der Pauw Hall Effect measurements with pressed-on In contacts and an error of $\pm 5\%$ was assumed in all electrical measurements. High-resolution cross-sectional transmission electron microscopy (HR-XTEM) was used to study the structure of both as-implanted and annealed specimens; all TEM specimens were prepared using focused ion beam-based techniques as described elsewhere.^{10,11} Rutherford backscattering with channeling (RBS/C) was also performed on as-implanted specimens to further characterize the damage resulting from ion-implantation. Finally, secondary ion mass spectrometry (SIMS) was performed on the as-implanted specimens to determine the implanted Si concentration profiles to allow determination of the active Si concentration in conjunction with electrical characterization.

Figs. 1(a)–1(e) show HR-XTEM images of as-implanted $\text{In}_{0.53}\text{Ga}_{0.47}\text{As}$ for implantation temperatures of 20–300 °C. In the case of implantation at 20 °C, an amorphous (α) layer extending ~ 30 nm from the surface of the specimen was evident in HR-XTEM, as shown in Fig. 1(a). However, for implantation temperatures of 80, 140, 200, and 300 °C, HR-XTEM did not reveal the presence of an α - $\text{In}_{0.53}\text{Ga}_{0.47}\text{As}$ layer as shown in Figs. 1(b)–1(e), respectively. Thus, an implant temperature greater than 80 °C was sufficient to prevent amorphization during the implantation for the implant conditions used in this study. HR-XTEM was also performed on specimens after annealing at 750 °C for 5 s using RTA as shown in Figs. 1(f)–1(j) to investigate the influence of

^{a)}Author to whom correspondence should be addressed. Electronic mail: aglind@ufl.edu.

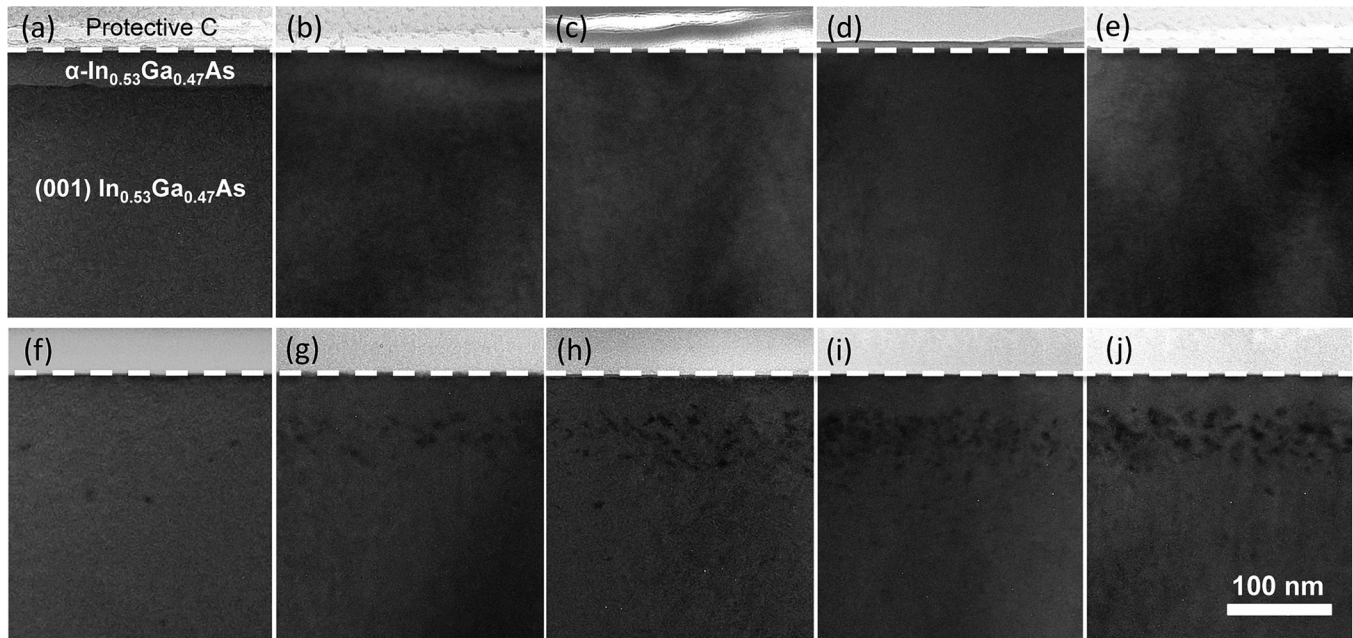


FIG. 1. HR-XTEM images of $\text{In}_{0.53}\text{Ga}_{0.47}\text{As}$ specimens Si^+ -implanted at 20 keV to a dose of $6.0 \times 10^{14} \text{ cm}^{-2}$: as-implanted for implantation temperatures of (a) 20, (b) 80, (c) 140, (d) 200, and (e) 300 °C and after annealing at 750 °C for 5 s using RTA for implantation temperatures of (f) 20, (g) 80, (h) 140, (i) 200, and (j) 300 °C; the surface of the specimens is indicated by the dashed lines.

implantation temperature on the resultant microstructure following annealing. For implantation temperatures of 20, 80, 140, 200, and 300 °C, shown in Figs. 1(f)–1(j), respectively, the microstructures of the annealed specimens each exhibit a single crystal microstructure indicating the $\alpha\text{-In}_{0.53}\text{Ga}_{0.47}\text{As}$ layer observed in the as-implanted state for an implantation temperature of 20 °C was completely re-grown as a result of subsequent annealing. For the case of an implantation temperature of 20 °C, type-II dislocation loops¹² near the initial α /crystalline interface were observed with an estimated planar density of $\sim 1.1 \times 10^{11} \text{ cm}^{-2}$, and no stacking faults or twins were observed in the initial $\alpha\text{-In}_{0.53}\text{Ga}_{0.47}\text{As}$ region crystallized by solid-phase epitaxial growth (SPEG). For the higher implantation temperatures (≥ 80 °C), sub-threshold type-I¹² dislocation loops were observed with an estimated planar density of $\sim 9.0 \times 10^{11} \text{ cm}^{-2}$.

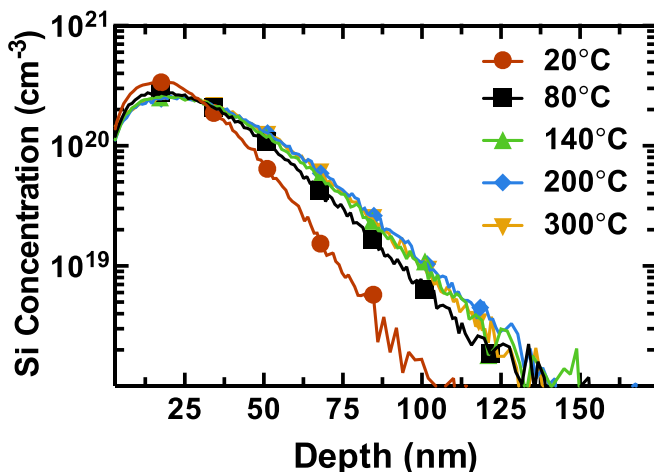


FIG. 2. As-implanted Si concentration profiles for $\text{In}_{0.53}\text{Ga}_{0.47}\text{As}$ specimens Si^+ -implanted at 20 keV to a dose of $6.0 \times 10^{14} \text{ cm}^{-2}$ at implantation temperatures of 20–300 °C as determined by SIMS.

Fig. 2 shows the as-implanted Si concentration profiles for different implantation temperatures as measured using SIMS. The Si concentration profiles for implantation temperatures greater than 140 °C were nearly indistinguishable. However, it is evident that the Si concentration profile is slightly shallower for an implantation temperature of 80 °C, while for an implantation temperature of 20 °C, the profile is significantly shallower. It should be noted that profile broadening due to thermal diffusion is reasonably assumed negligible given the reported diffusivity of Si in $\text{In}_{0.53}\text{Ga}_{0.47}\text{As}$ (Ref. 9) as well as the nearly identical Si profiles observed for implantation temperatures of 140 to 300 °C. However, profile broadening may be reasonably attributed to channeling and/or radiation-enhanced diffusion effects. In the case of channeling, a reduction in random channeling will occur due to amorphization and as well as an increase in point defects for implantation temperatures of 20 and 80 °C, respectively. Likewise, radiation enhanced diffusion is also plausible given previous results showing similar profile broadening of Se^+ -implantation in GaAs at elevated temperatures.¹³ As the possible reasons for profile broadening notwithstanding, it should be noted that the determination of Si profiles was of primary importance for determination of Si solubility, as will be discussed subsequently, rather than providing any direct structural information.

RBS/C analysis was performed on the as-implanted specimens to investigate the disorder to the crystal lattice as a function of implantation temperature. As shown in Fig. 3, it is evident that the backscattering yield is greatest for an implantation temperature of 20 °C, which is consistent with the amorphization observed in HR-XTEM presented in Fig. 1(a). However, it is also evident that the backscattered yield is also slightly greater for an implantation temperature of 80 °C as compared to higher implantation temperatures, which suggests that for all implantation temperatures greater

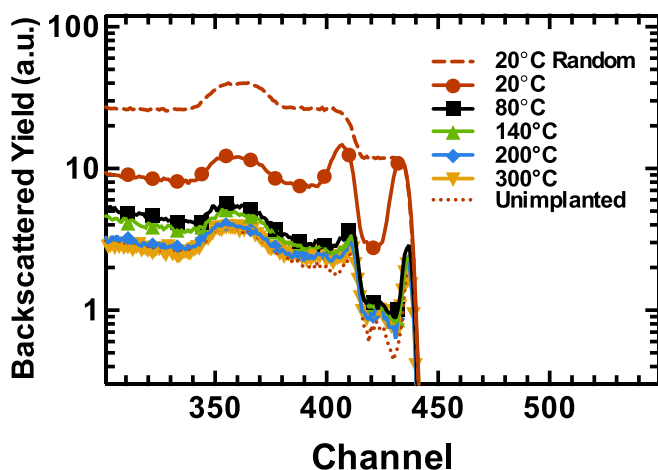


FIG. 3. RBS/C spectra showing the backscattered yield versus channel number for $\text{In}_{0.53}\text{Ga}_{0.47}\text{As}$ specimens Si^+ -implanted at 20 keV to a dose of $6.0 \times 10^{14} \text{ cm}^{-2}$ at implantation temperatures of 20–300 °C.

than or equal to 80 °C, amorphization was avoided (as per Figs. 1(b)–1(e)), but the disorder in the crystal lattice was greatest for an implantation temperature of 80 °C.

The active Si sheet number (N_s) and mobility (μ) as a function of implantation temperature are presented in Fig. 4. For implantation temperatures ≥ 80 °C (where amorphization was avoided), N_s decreased with increasing implantation temperature. N_s was at a maximum for an implantation temperature of 80 °C, which is the minimum temperature shown to avoid amorphization. An implantation temperature of 80 °C also yielded a maximum activation efficiency of $\sim 15\%$ indicating that a large fraction of the implanted dose remained inactive after annealing. An estimated Si solubility of $\sim 9.4 \times 10^{18} \text{ cm}^{-3}$ for the implantation temperature of 80 °C was calculated based on the active sheet number in conjunction with the measured Si profile as determined by SIMS as described elsewhere.¹⁴ It was reasonably assumed that no Si profile motion occurred as a result of annealing as per extensive prior results showing the very low diffusivity of Si in $\text{In}_{0.53}\text{Ga}_{0.47}\text{As}$ for annealing temperatures < 750 °C.^{9,15,16} The calculated Si solubility of $9.4 \times 10^{18} \text{ cm}^{-3}$ for the implantation temperature of 80 °C agrees well with the previous work studying the solubility of Si in $\text{In}_{0.53}\text{Ga}_{0.47}\text{As}$.^{5,16,17} The diminishing decrease in activation with increasing implantation temperature for implantation temperatures greater than

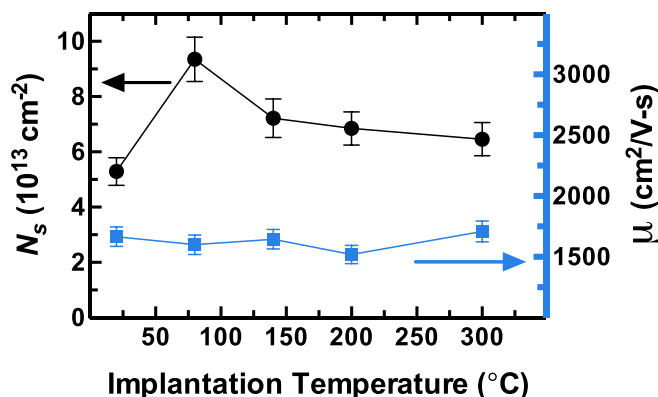


FIG. 4. Active sheet number (N_s) and mobility (μ) of $\text{In}_{0.53}\text{Ga}_{0.47}\text{As}$ specimens Si^+ -implanted at 20 keV to a dose of $6.0 \times 10^{14} \text{ cm}^{-2}$ after annealing at $T = 750$ °C for 5 s using RTA as a function of implantation temperature.

80 °C still results in higher overall activation for an implantation temperature of 300 °C than for an implantation temperature of 20 °C, which is consistent with the previous studies which showed that elevated implantation temperatures will show activation improvements over doses that are likely amorphizing at room temperature.^{5,6} Interestingly, the mobility does not show any significant dependence on active sheet number for the implant conditions studied; as a result, the measured sheet resistance as a function of implantation temperature demonstrates an inversely proportional relationship to sheet number with a minimum measured sheet resistance of $41 \Omega/\square$ for an implantation temperature of 80 °C. Results by Alian *et al.*⁹ similarly show no clear dependence of mobility on active sheet number for similar implantation conditions and levels of electrical activation, which suggests that mobility is not dominated by ionized impurity scattering for shallow implantation of Si^+ to large doses when electrical activation is low. The origin of the observed insensitivity of mobility to active sheet number is unclear at this point, but due to the shallow nature of the implantation profile, one possibility may be that mobility is limited by surface scattering.

The results from HR-XTEM, SIMS, and RBS/C suggest the methodology for achieving the greatest activation of Si in ion-implanted $\text{In}_{0.53}\text{Ga}_{0.47}\text{As}$ is to perform ion implantation such that the material remains crystalline, but acquires a large amount of damage from the implanted Si^+ in the form of point defects. Simply stated, Si activation is maximized when non-amorphizing damage due to Si^+ implantation is also maximized. The introduction of point defects presumably provides sites (Ga, In vacancies) for substitutional incorporation of Si to occur upon annealing, thus producing n-type doping. As a result, there is shown to be no benefit to performing Si^+ implantation at temperatures any higher than is necessary to avoid amorphization. The poor activation observed for an implantation temperature of 20 °C (where amorphization occurred) may be a result of differences in Si incorporation in the point defect rich region behind the amorphous-crystalline interface and Si incorporation occurring from SPEG, which is necessary to re-crystallize the amorphized layer. In fact, similar results were demonstrated in Si^+ -implanted GaAs, where it was shown that Si activation during SPEG was basically negligible.¹⁸

In conclusion, the role of specimen temperature during ion-implantation on the activation of Si in $\text{In}_{0.53}\text{Ga}_{0.47}\text{As}$ was studied. It was shown using a combination of HR-XTEM, SIMS, and RBS that for Si^+ implantation temperatures less than 80 °C amorphization occurred while for implantation temperatures of 80 °C or greater, amorphization was avoided but damage to the crystal lattice decreased with increasing implantation temperature. Hall effect measurements also revealed that activation was maximized for an implantation temperature of 80 °C, with activation decreasing with increasing implantation temperature. The results of HR-XTEM and RBS/C suggest that the key to maximizing activation of ion-implanted Si in $\text{In}_{0.53}\text{Ga}_{0.47}\text{As}$ is to create the greatest amount of damage to the crystal lattice during the implantation of Si while avoiding amorphization. This implantation temperature-dependent enhancement in activation is presumably the result of creating a large concentration

of point defects such that the ion-implanted Si has sufficient sites for activation upon annealing.

The authors acknowledge the Semiconductor Research Corporation for funding this work. The Major Analytical Instrumentation Center at the University of Florida is acknowledged for use of the transmission electron microscopy and focused ion beam facilities.

¹M. Heyns and W. Tsai, *MRS Bull.* **34**, 485 (2009).

²J. A. del Alamo, *Nature* **479**, 317 (2011).

³T. Pearsall, *IEEE J. Quantum Electron.* **16**, 709 (1980).

⁴M. V. Rao, *Nucl. Instrum. Methods Phys. Res. B* **79**, 645 (1993).

⁵T. Penna, B. Tell, A. S. H. Liao, T. J. Bridges, and G. Burkhardt, *J. Appl. Phys.* **57**, 351 (1985).

⁶J. P. Donnelly, W. T. Lindley, and C. E. Hurwitz, *Appl. Phys. Lett.* **27**, 41 (1975).

⁷B. Tell, K. F. Brown-Goebeler, and C. L. Cheng, *Appl. Phys. Lett.* **52**, 299 (1988).

⁸T. E. Haynes, W. K. Chu, and S. T. Picraux, *Appl. Phys. Lett.* **50**, 1071 (1987).

⁹A. Alian, G. Brammertz, N. Waldron, C. Merckling, G. Hellings, H. C. Lin, W. E. Wang, M. Meuris, E. Simoen, K. De Meyer, and M. Heyns, *Microelectron. Eng.* **88**, 155 (2011).

¹⁰L. A. Giannuzzi and F. A. Stevie, *Micron* **30**, 197 (1999).

¹¹M. Sugiyama, *J. Electron Microsc.* **53**, 527 (2004).

¹²K. S. Jones, S. Prussin, and E. R. Weber, *Appl. Phys. A.* **45**, 1 (1988).

¹³A. Lidow, J. F. Gibbons, V. R. Deline, and C. A. Evans, *Appl. Phys. Lett.* **32**, 149 (1978).

¹⁴A. Satta, E. Simoen, T. Clarysse, T. Janssens, A. Benedetti, B. De Jaeger, M. Meuris, and W. Vandervorst, *Appl. Phys. Lett.* **87**, 172109 (2005).

¹⁵E. Hailemariam, S. J. Pearton, W. S. Hobson, H. S. Luftman, and A. P. Perley, *J. Appl. Phys.* **71**, 215 (1992).

¹⁶M. V. Rao, S. M. Gulwadi, P. E. Thompson, A. Fathimulla, and O. A. Aina, *J. Electron. Mater.* **18**, 131 (1989).

¹⁷H. Kawata, H. Nishi, Y. Bamba, T. Sakurai, and H. Hashimoto, *Jpn. J. Appl. Phys., Part 2*, **21**, L431 (1982).

¹⁸W. G. Opyd, J. F. Gibbons, and A. J. Mardinly, *Appl. Phys. Lett.* **53**, 1515 (1988).